Proceedings of the 30th International Cosmic Ray Conference
Rogelio Caballero, Juan Carlos D'Olivo, Gustavo Medina-Tanco,
Lukas Nellen, Federico A. Sánchez, José F. Valdés-Galicia (eds.)
Universidad Nacional Autónoma de México,
Mexico City, Mexico, 2008
Vol. 1 (SH), pages 593–596

30TH INTERNATIONAL COSMIC RAY CONFERENCE

Implication of the sidereal anisotropy of ~5 TeV cosmic ray intensity observed with the Tibet III air shower array

THE TIBET ASγ COLLABORATION
M. AMENOMORI[1], X. J. BI[2], D. CHEN[3], S. W. CUI[4], DANZENGLUOBU[5], L. K. DING[2], X. H. DING[5], C. FAN[6], C. F. FENG[6], ZHAOYANG FENG[2], Z. Y. FENG[7], X. Y. GAO[8], Q. X. GENG[8], H. W. GUO[5], H. H. HE[2], M. HE[6], K. HIBINO[9], N. HOTTA[10], HAIBING HU[5], H. B. HU[2], J. HUANG[11], Q. HUANG[7], H. Y. JIA[7], F. KAJINO[12], K. KASAHARA[13], Y. KATAYOSE[3], C. KATO[14], K. KAWATA[11], LABACIREN[5], G. M. LE[15], A. F. LI[6], J. Y. LI[6], Y.-Q. LOU[16], H. LU[2], S. L. LU[2], X. R. MENG[5], K. MIZUTANI[13,17], J. MU[8], K. MUNAKATA[14], A. NAGAI[18], H. NANJO[1], M. NISHIZAWA[19], M. OHNISHI[11], I. OHTA[20], H. ONUMA[17], T. OUCHI[9], S. OZAWA[11], J. R. REN[2], T. SAITO[21], T. Y. SAITO[22], M. SAKATA[12], T. K. SAKO[11], M. SHIBATA[3], A. SHIOMI[9,11], T. SHIRAI[9], H. SUGIMOTO[23], M. TAKITA[11], Y. H. TAN[2], N. TATEYAMA[9], S. TORII[13], H. TSUCHIYA[24], S. UDO[11], B. WANG[8], H. WANG[2], X. WANG[11], Y. WANG[2], Y. G. WANG[6], H. R. WU[2], L. XUE[6], Y. YAMAMOTO[12], C. T. YAN[11], X. C. YANG[8], S. YASUE[25], Z. H. YE[15], G. C. YU[7], A. F. YUAN[5], T. YUDA[9], H. M. ZHANG[2], J. L. ZHANG[2], N. J. ZHANG[6], X. Y. ZHANG[6], Y. ZHANG[2], YI ZHANG[2], ZHAXISANGZHU[5] AND X. X. ZHOU[7]
[1]Department of Physics, Hirosaki University, Hirosaki 036-8561, Japan. [2]Key Laboratory of Particle Astrophysics, Institute of High Energy Physics, Chinese Academy of Sciences, Beijing 100049, China. [3]Faculty of Engineering, Yokohama National University, Yokohama 240-8501, Japan. [4]Department of Physics, Hebei Normal University, Shijiazhuang 050016, China. [5]Department of Mathematics and Physics, Tibet University, Lhasa 850000, China. [6]Department of Physics, Shandong University, Jinan 250100, China. [7]Institute of Modern Physics, SouthWest Jiaotong University, Chengdu 610031, China. [8]Department of Physics, Yunnan University, Kunming 650091, China. [9]Faculty of Engineering, Kanagawa University, Yokohama 221-8686, Japan. [10]Faculty of Education, Utsunomiya University, Utsunomiya 321-8505, Japan. [11]Institute for Cosmic Ray Research, University of Tokyo, Kashiwa 277-8582, Japan. [12]Department of Physics, Konan University, Kobe 658-8501, Japan. [13]Research Institute for Science and Engineering, Waseda University, Tokyo 169-8555, Japan. [14]Department of Physics, Shinshu University, Matsumoto 390-8621, Japan. [15]Center of Space Science and Application Research, Chinese Academy of Sciences, Beijing 100080, China. [16]Physics Department and Tsinghua Center for Astrophysics, Tsinghua University, Beijing 100084, China. [17]Department of Physics, Saitama University, Saitama 338-8570, Japan. [18]Advanced Media Network Center, Utsunomiya University, Utsunomiya 321-8585, Japan. [19]National Institute of Informatics, Tokyo 101-8430, Japan. [20]Tochigi Study Center, University of the Air, Utsunomiya 321-0943, Japan. [21]Tokyo Metropolitan College of Industrial Technology, Tokyo 116-8523, Japan. [22]Max-Planck-Institut f\"ur Physik, M\"unchen D-80805, Deutschland. [23]Shonan Institute of Technology, Fujisawa 251-8511, Japan. [24]RIKEN, Wako 351-0198, Japan. [25]School of General Education, Shinshu University, Matsumoto 390-8621, Japan.
kmuna00@gipac.shinshu-u.ac.jp

Abstract: We show that the large-scale anisotropy of ~5 TeV galactic cosmic ray (GCR) intensity observed by Tibet Air Shower experiment can be reproduced by the superposition of a bi-directional and uni-directional flows (BDF and UDF) of GCRs. The heliosphere is located inside the local interstellar cloud (LIC) very close to the inner edge of the LIC. If the GCR population is lower inside the LIC than outside, the BDF flow is expected from the parallel diffusion of GCRs into LIC along the local interstellar magnetic field (LISMF) connecting the heliosphere with the region outside the LIC, where the GCR population is higher. A type of the UDF, on the other hand, is expected from the $\mathbf{B}\times\nabla N$ drift flux driven by a gradient of GCR density (N) in the LISMF (**B**). The LISMF orientation deduced from

the best-fit direction of the BDF is almost parallel to the galactic plane and more consistent with the suggestion of Frisch (1996) than that of Lallement et al. (2005). We note that the model gives the information on the LISMF polarity together with its orientation.

Introduction

In this paper, we analyze the sidereal anisotropy of ~5 TeV GCR intensity observed by the Tibet Air Shower (AS) experiment, which is currently the world's most precise measurement of GCR intensity in this energy region, utilizing both the high count rate and good angular resolution of the incident direction of the primary GCR. The GCR anisotropy in this energy region is free from the solar modulation, while it is still sensitive to the local magnetic field structure with a spatial scale comparable to the Larmor radius of the observed GCR, which is about 0.005 pc or 1000 AU for 5 TeV protons in a 1 μG interstellar magnetic field. The sky-map of the directional intensity recently reported by the Tibet AS experiment clearly showed the large-scale feature observed with the statistical significance of more than 10 σs [1]. The contribution of primary gamma rays to this large-scale anisotropy should be small, as the similar feature is also reported from a deep-underground muon measurement, which has only negligible response to the primary gamma rays [2]. This large-scale feature seems to be almost independent of the GCR energy over a range from multi-TeV up to ~100 TeV.

Analysis and Results

The Tibet III Air Shower Array experiment has been conducted at Yangbajing (90.522°E, 30.102° N; 4300 m above sea level) in Tibet, China. The array composed of 533 scintillation counters of 0.5 m^2 each covers a detection area of 22,050 m^2 achieving a trigger rate of ~680 Hz. GCR events are selected for analyses, if any four-fold coincidence occurs in the counters with each recording more than 0.8 particles in charge, if the air shower core position is located in the array, and if the zenith angle of arrival direction is ≤45°. With all these criteria, the array has the modal GCR energy of ~5 TeV. The angular resolution of the arrival direction of each shower is estimated to be ~0.9° from Monte Carlo simulations and was verified by measuring the Moon's shadow in GCRs [3]. In this paper, we analyze a total of ~37 billion air shower events recorded in 1318.9 live days from November 1999 to October 2005. For each short time step (e.g., 2 min), we analyze shower event number in each zenith angle belt and subtract the average in the belt from the intensity in each azimuth bin. By this subtraction, we can eliminate the atmospheric effect, which is common for all azimuth bins in each zenith angle belt. This calculation is then extended step by step to all points in the surveyed sky (see [4] for details of data analysis). Since the shower rate largely varies according to the zenith angle of the arrival direction, the absolute GCR intensities in different declination belts cannot be compared. Thus, the average intensity in each declination

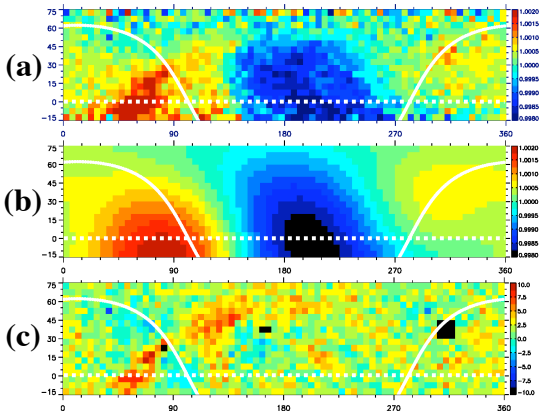

Figure 1: GCR intensity in 5°×5° pixel represented in a color coded format as a function of the right ascension and the declination. The saturation occurs at ±0.2 % for the intensity map and ± 10 σs for the significance map. (a): observed anisotropy, (b): reproduced anisotropy, (c): significance map of the residual anisotropy. The broken line in each panel shows the celestial equator, while the white represents the Galactic equator. The black pixels in (c) containing strong TeV γ-ray sources are excluded from the best-fit analysis.

belt is normalized to unity.

Figure 1(a) shows the normalized GCR intensity in 5°×5° pixels in a color-coded format as a function of the right ascension (α) on the horizontal axis and the declination (δ) on the vertical axis. This sky-map covers 360° of α, but covers only 90° of δ ranging from -15° to +75° due to the event selection criterion limiting zenith angles to ≤45°. The map clearly shows a large-scale anisotropy, consisting of a ~0.2 % excess (around α~90° and δ~−10°) and a ~0.2 % deficit (around α~180° and δ~0°), each observed with a statistical significance more than 10 σs [1]. We note that the observed angular separation between the excess and the deficit is only ~120°, which is much smaller than 180° expected from a uni-directional flow (UDF) but significantly larger than 90° expected from a bi-directional flow (BDF). Only a combination of the uni-directional and bi-directional flows can achieve a reasonable fit to the observed anisotropy. From this point, we perform the best-fit calculation to the observed

anisotropy with a model intensity $I_{n,m}$ in n-th right ascension and m-th declination pixel expressed, as

$$\begin{aligned} I_{n,m} = {} & a_{1\perp}\cos\chi_1(n,m:\alpha_1,\delta_1) \\ & + a_{1//}\cos\chi_2(n,m:\alpha_2,\delta_2) \\ & + a_2\cos^2\chi_2(n,m:\alpha_2,\delta_2) \end{aligned} \qquad (1)$$

where $a_{1\perp}$ and $a_{1//}$ are amplitudes of UDFs, a_2 is the amplitude of the BDF, (α_1, δ_1) and (α_2, δ_2) are right ascensions and declinations of the reference axes of the UDF and BDF, respectively, and χ_1 (χ_2) is the angle between the center of each pixel and the reference axis of UDF (BDF). We assume that two reference axes are perpendicular to each other, according to our physical interpretation of the UDF and BDF, as will be described later. We first normalize the average of $I_{n,m}$ in each declination belt to unity and get the normalized model intensity $i_{n,m}$, just same as we did for the observed data to produce Figure 1(a). By comparing $i_{n,m}$ with the observed intensity $i^{obs}_{n,m}$, we obtain six best-fit parameters ($a_{1\perp}$, $a_{1//}$, a_2, α_1, α_2, δ_2) minimizing the residual S defined, as

$$S = \sum_{n=1}^{72}\sum_{m=1}^{18} s^2_{n,m} = \sum_{n=1}^{72}\sum_{m=1}^{18} (i^{obs}_{n,m} - i_{n,m})^2 / \sigma^2_{n,m} \qquad (2)$$

where $\sigma_{n,m}$ is the statistical error of the intensity in each pixel.

Figure 1(b) shows the best-fit $i_{n,m}$, while Figure 1(c) shows the residual $s_{n,m}$ in each pixel. It is seen that the large-scale anisotropy in Figure 1(a) is well reproduced even with such a simple model. The residual $s_{n,m}$ in Figure 1(c), on the other hand, indicates that the "skewed" structure of the excess in Figure 1(a) needs to be modeled further. The minimum S-value in (2) divided by the degree of freedom (72×18-6=1290) is as large as 2.5, mainly due to the "skewed" structure not reproduced properly.

Implication of the Model Anisotropy

As mentioned earlier in this paper, the directional anisotropy of the GCR intensity is most sensitive to the magnetic structure with the spatial scale comparable to the Larmor radius of GCRs. The Larmor radius of 0.005 pc for 5 TeV GCRs is much larger than the size of the heliosphere, but significantly smaller than the size of the Galactic arms of the order of 100 pc. An intermediate structure called the Local Interstellar Cloud (LIC) has been reported from the optical measurement of the interstellar absorption lines recorded in the spectra of nearby stars [5]. The LIC is an egg-shaped cloud of the size of ~5 pc and filled with the relatively warm interstellar gas. The heliosphere is located inside the LIC very close to the inner edge of the LIC. Outside the LIC sweeping past the heliosphere at a speed of 26 km/s, there is another cloud called G-cloud moving toward the heliosphere at a slightly higher speed of 29 km/s. It is also suggested that the local interstellar magnetic field (LISMF) surrounding the heliosphere could be compressed between the two cloudlets [6]. The minimum distance to the LIC edge from the heliosphere is estimated as small as ~0.1 pc. It

is possible, therefore, that the observed anisotropy is governed by the LISMF and the local gradient of the GCR density (or population) in the LIC.

According to our preliminary best-fit analysis described above, the large-scale anisotropy can be reproduced with a combination of the UDF and BDF. We suggest that such flows may be expected if the GCR density is lower inside the LIC than outside, for instance, due to an adiabatic expansion of the LIC surrounded by the large-scale galactic magnetic field. If this is the case, the BDF (with an amplitude of a_2) is expected from the pitch angle diffusion of GCRs into LIC along the LISMF line connecting the heliosphere on its both ends with the region outside the LIC, where the GCR density is higher. The reference axis of the BDF (α_2, δ_2) is parallel to the LISMF lines. The parallel diffusion along the LISMF also causes a UDF (with an amplitude of $a_{1//}$) along the LISMF. On the other hand, another UDF ($a_{1\perp}$) is also expected from the drift anisotropy, which is expressed as a vector product ($\mathbf{B}\times\mathbf{G}$) between the LISMF vector ($\mathbf{B}$) and the density gradient vector ($\mathbf{G}$). The reference axis of this type of UDF (α_1, δ_1) is, therefore, perpendicular to $\mathbf{B}$ and (α_2, δ_2), as modeled in Equation (1). The directions of the LISMF and the perpendicular UDF derived from the present model are listed in Table 1 together with $a_{1\perp}$, $a_{1//}$ and a_2 and indicated in Figure 2 showing the best-fit anisotropy ($I_{n,m}$) in the Galactic coordinate. In Figure 2, the direction of LISMF derived from the present model is compared with that suggested by [6] and [7]. The LISMF direction we obtain is more parallel to the Galactic plane, favoring the direction report by Frisch [7]. We add to note that the model, if holds, yields the polarity of the LISMF together with its orientation.

Table 1: Best-fit parameters in Equation (1). Two numbers in each brace are the Galactic longitude and latitude of the reference axis.

$a_{1\perp}$ (%)	$a_{1//}$ (%)	a_2 (%)
0.108	0.096	0.142

α_1, δ_1 (°)	α_2, δ_2 (°)
357.5, - 22.5 (49.7, -75.6)	97.4, -22.5 (232.0, -14.4)

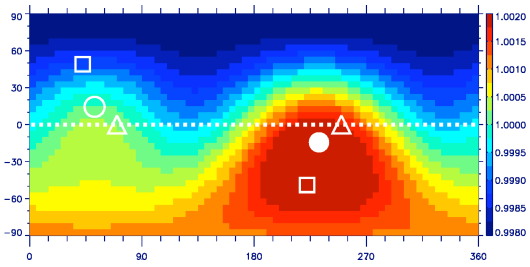

Figure 2: The best-fit in the Galactic coordinate. Full (open) circle represents the direction parallel (anti-parallel) to the LISMF derived from the present analysis. Squares and triangles show the LISMF orientations by [6] and [7]. Note that the intensity at the northern high-latitude is lower than the intensity at the southern high-latitude due to the perpendicular UDF.

Acknowledgements

The collaborative experiment of the Tibet Air Shower Arrays has been performed under the auspices of the Ministry of Science and Technology of China and the Ministry of Foreign Affairs of Japan.

References

[1] M. Amenomori et al., *Science*, 314:439, 2006.
[2]G . Guillian et al., *Phys. Rev. D*, 7:062003-1, 2007.
[3] M. Amenomori et al., *Phys. Rev. D*, 47:2675, 1993.
[4] M. Amenomori et al., *Astrophys. J.*, 633:1005, 2005.
[5] S. Redfield and J. L. Linsky, *Astrophys. J.*, 534:825, 2000.
[6] R. Lallement et al., *Science*, 307:1447, 2005.
[7] P. C. Frisch, *Space Sci. Rev.*, 78:213, 1996.